www.lpr-journal.org Vol. 7 No. 1 January 2013

LASER & PHOTONICS REVIEWS

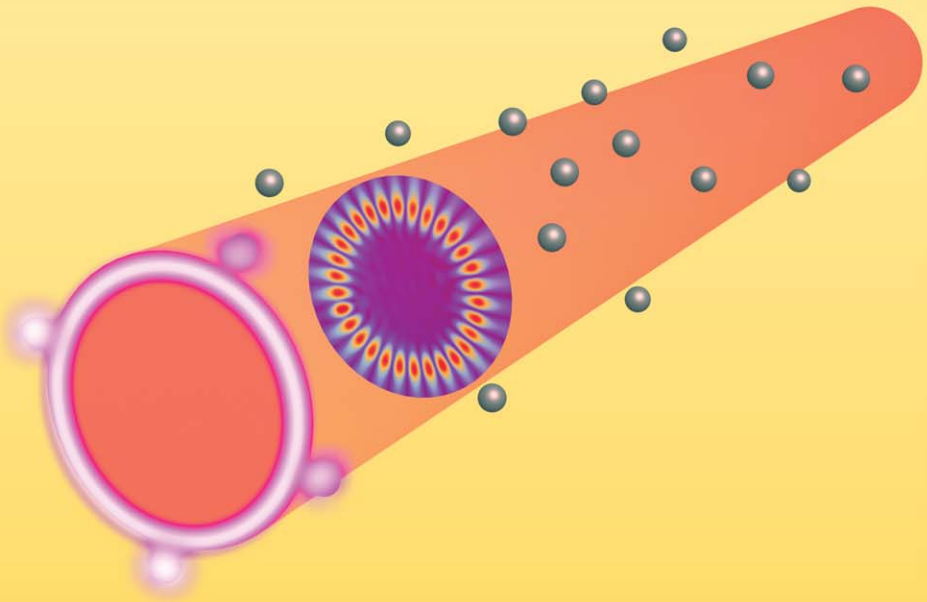

Whispering gallery mode microlasers and refractive index sensing based on single polymer fiber

The realization of whispering gallery mode (WGM) lasing in polymer fibers is hindered by an appropriate method to dissolve the polymer and the gain material. In this work by **Van Duong Ta et al.** (**pp. 133–139**), microfibers fabricated by directly drawing from a dye doped polymer solution are exhibited as high quality microlasers and microsensors. Multimode and even single-mode lasing is observed from the fiber under optical pumping at room temperature. The linewidth of lasing mode is narrower than 0.09 nm. The lasing mechanism is unambiguously verified by comprehensive spectroscopic analysis and ascribed to WGMs. Diameter- and polarization-dependent lasing characteristics are systematically investigated, showing good agreement with the theoretical calculation. Particularly, application of the fiber laser for refractive index sensing based on resonant shift of lasing mode is demonstrated and the sensitivity up to about 300 nm/RIU is achieved. The promising potential of high quality polymer microfibers as optical sensors and multi-function components for flexible photonic integrated systems is highly expected.

Picture: Whispering gallery mode (WGM) lasing emission (bright ring) is realized from a dye-doped polymer microfiber. This microlaser can serve as refractive index sensing of tetrahydrofuran (THF) solution based on the interaction of the THF molecules (solid spheres) with evanescent wave of WGM modes. The simulated field distribution of WGMs is inserted inside the fiber.

WILEY-VCH

Laser Photonics Rev. **7,** No. 1, 133–139 (2013) / **DOI** 10.1002/lpor.201200074

LASER & PHOTONICS REVIEWS

Abstract The realization of whispering gallery mode (WGM) lasing in polymer fibers is hindered by an appropriate method to dissolve the polymer and the gain material. In this work, microfibers fabricated by directly drawing from a dye doped polymer solution are exhibited as high quality microlasers and microsensors. Multi-mode and even single-mode lasing is observed from the fiber under optical pumping at room temperature. The linewidth of lasing mode is narrower than 0.09 nm. The lasing mechanism is unambiguously verified by comprehensive spectroscopic analysis and ascribed to WGMs. Diameter- and polarization-dependent lasing characteristics are systematically investigated, showing good agreement with the theoretical calculation. Particularly, application of the fiber laser for refractive index sensing based on resonant shift of lasing mode is demonstrated and the sensitivity up to about 300 nm/RIU is achieved. The promising potential of high quality polymer microfibers as optical sensors and multi-function components for flexible photonic integrated systems is highly expected.

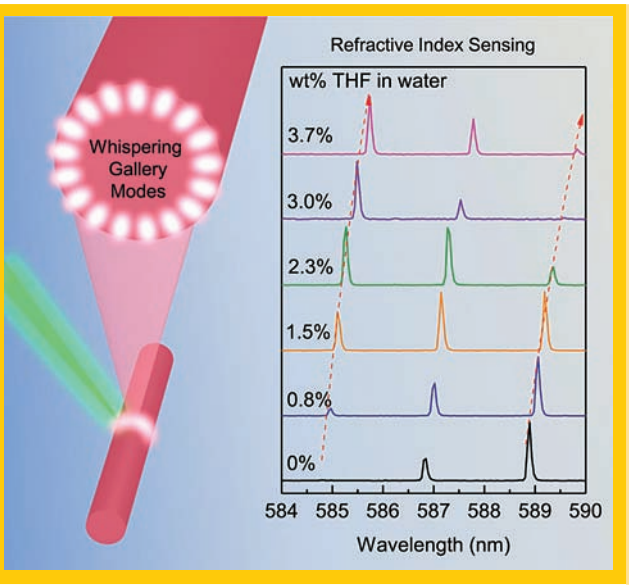

ORIGINAL PAPER

Whispering gallery mode microlasers and refractive index sensing based on single polymer fiber

Van Duong Ta[1], Rui Chen[1], Lin Ma[1], Yong Jun Ying[1], and Han Dong Sun[1,2,*]

1. Introduction

The development of low-dimensional photonic nano/micro structures, being the building blocks for single-chip technologies, has attracted intensive research interest [1–4]. Due to the low cost and the mechanical flexibility, organic materials are considered to be a promising candidate for flexible photonic circuits [5–7]. Among various kinds of organic nano/microstructures, polymer fibers can be readily fabricated by approaches such as electrospinning deposition [8–12], directly drawing from liquid polymer solution or melt [13–18], or vapor deposition polymerization [19], which have been employed for sub-wavelength waveguides, light-emitting sources, optical sensors, etc. Recently, polymer fibers have been demonstrated successfully for creation of inverters and multiplexers for digital logic [20], which reveals their potential application in micro/nanophotonic integrated system.

While low-threshold laser source is important for optoelectronic integrated system, only few works have realized optical nano/micro resonators based on polymer fibers, characterized by the observation of laser emission from a piece of conjugated or dye-doped polymer fiber [12,21]. In these structures, the two cutting edges of the fiber are served as mirrors and formed the so called Fabry-Pérot (F-P) or one-dimensional (1D) cavity where light is amplified to achieve the stimulated emission. However, the quality (Q) factor of F-P cavity is low due to the high optical losses at the fiber's edges. To overcome this drawback, other kinds of microcavity in high quality fiber should be investigated.

Generally speaking, microfibers possess cylindrical shape with circular cross-sections, which has high potential to form the so-called whispering gallery modes (WGMs). It is known that the WGM cavity has essentially a high Q factor and a small mode volume, therefore, is appropriate for low-threshold lasers [22,23]. WGM lasing has been investigated from cylindrical microresonators based on capillary tubes [24], microdisks [25–27], and microrings [26,27]. For the organic material, a polymer microdisk can be fabricated by photolithographycally etched from a thin film [26,27], while for the microrings, the WGM lasing was obtained by coating an active thin film around the optical fiber [26,27]. Very recently, a 3D microlaser has been demonstrated from electrospun polymer microfibers but the rough outer surface of these fibers might lead to considerable optical losses due to the scattering [28].

[1] Division of Physics and Applied Physics, School of Physical and Mathematical Sciences, Nanyang Technological University, Singapore 637371, Singapore
[2] Centre for Disruptive Photonic Technologies (CDPT), Nanyang Technological University, Singapore
*Corresponding author(s): e-mail: hdsun@ntu.edu.sg

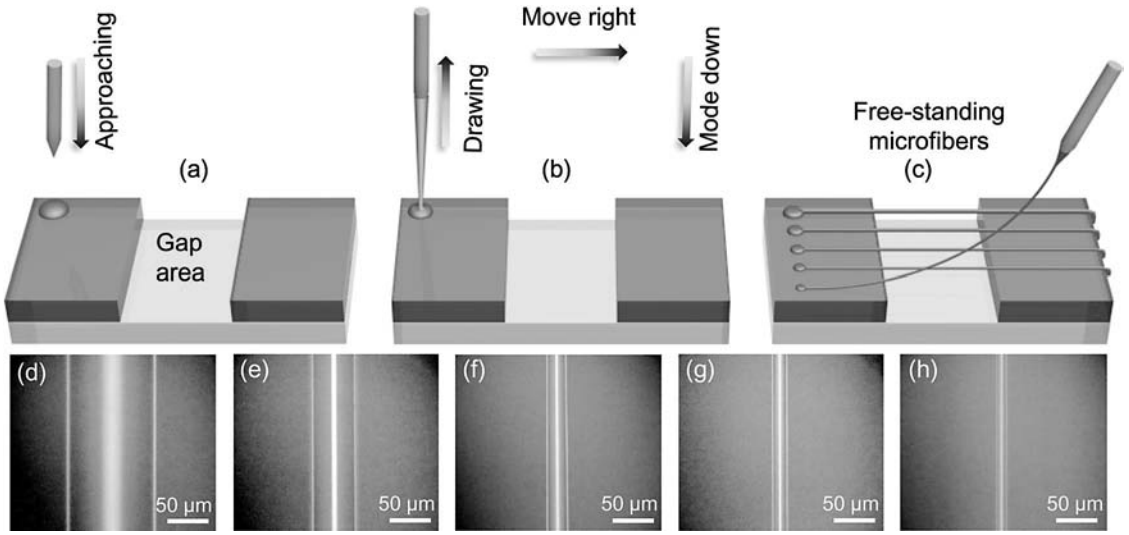

Figure 1 (online color at: www.lpr-journal.org) (a)–(c) Schematic diagrams demonstrates fabrication of microfiber by direct drawing from dye-doped polymer solution. The gap is around 0.5 cm. (d)–(h) The top-down view optical image of microfibers with different sizes under halogen illumination.

In this work, we demonstrate the WGM lasing from high quality, direct drawing, and flexible polymer microfibers. The diameters of microfibers range from 5 to 100 μm, fabricated with well and precise control. At room temperature, single and multi-mode lasing upon optical pumping are observed from dye-doped microfibers by using a microphotoluminescence (μ-PL) system. The proposed WGM lasing mechanism is experimentally verified by the analysis of i) lasing peaks and ii) the polarization dependence of the longitudinal modes, and further theoretically supported by the simulation using the finite element method. The cavity size dependence of lasing characteristics has also been systematically investigated. Application of the fiber for refractive index sensing is demonstrated with sensitivity up to about 300 nm per refractive index unit (RIU).

2. Fabrication and optical measurement

The solution used for microfiber fabrication was prepared as follows. First of all, polymethylmethacrylate (PMMA) was dissolved in dichloromethane with concentration about 11wt%. Then, Rhodamine 6G (R6G) and epoxy resin (Araldite® 506 from Sigma-Aldrich) [29] were subsequently added into the solvated PMMA. Ratio of PMMA and epoxy resin is ∼1:2 in weight, and concentration of R6G is around 0.06 wt%. Ultrasonic was used in each process for dispersing the solutes.

Figure 1 shows a schematic diagram of R6G doped microfiber fabricated by physically drawing from the composite solution, together with optical images of the obtained microfibers. It is important to note that in our work we have introduced the epoxy resin, which is semi-liquid and high viscous, into the solution. This material helps to increase the viscosity of the solution and also significant slows down the evaporation rate of solvent from the microfiber during the drawing process. As a result, microfibers with smooth outer surfaces, long lengths (up to 20 cm with high uniformity), and a wide range of tunable diameters can be obtained.

To create the microfibers, a solution droplet was deposited on the substrate (Fig. 1a), and a metal rod with a sharp tip (Figure S1c) was then approached vertically down and immersed into the droplet. After that, the rod tip was retracted from the droplet and the microfiber was formed by drawing at a constant speed (Fig. 1b) [14]. To fix the microfiber on the substrate for subsequent characterization, the rod was moved right and down to the edge of the substrate (Figs. 1b, c). As shown in the figure, the gap enables to obtain free-standing microfibers surrounded by air only, which is convenient for optical measurements. We are able to fabricate microfibers with different diameters by drawing with different speeds [30]. These microfibers were subsequently dried in air for structure stabilization. Figures 1d–h illuminate the optical images of solid-state microfibers with different sizes. The cross-section of a typical fiber was examined by a confocal microscopy image and the result indicates that the fiber has a circular cross-section (Fig. S1). In addition, the outer surface of our fibers is highly smooth, imaged by scanning electron microscopy (SEM) shown in Fig. S1.

Optical investigation of individual microfiber was carried out by using a μ-PL system (see Fig. S2 for more information) at room temperature. A beam from a frequency-doubled, *Q*-switched Nd:YAG laser (wavelength: 532 nm, pulse width: 1 ns, frequency: 60 Hz) was guided at an angle ∼45° to the normal of the XYZ translation stage. The excitation beam was then focused to excite the microfiber with elliptical spot of about 0.8 × 1.2 mm. In addition, the polarization of laser excitation is parallel to the fiber axis. PL was collected by an objective (50×, NA = 0.42)

which was delivered to a camera for PL image or coupled to a spectrometer equipped with a silicon charged coupled device (CCD) for spectra recoding (spectral resolution ~0.043 nm).

In principle, any variations in the refractive index of the medium surrounding the fiber wills lead to changes of optical path inside the fiber, therefore resulting in a slight shift in resonant mode. Based on this idea, demonstration of refractive index sensing of the fiber is presented. Firstly, the fiber is fixed on top of a Distributed Bragg Reflector (DBR) substrate [29]. Following, the DBR is also immobilized in a glass holder by using a double side tape. Finally, 23 ml of water is funneled into the holder. Tetrahydrofuran (THF) is used as a factor to increase refractive index of surrounding medium. The fiber needs to be fixed well to prevent its vibration in the liquid medium. The fiber is then optically pumped (the same as it is hold in the air) with a constant pump pulse energy (PPE). After recording the spectrum, 0.2 ml of THF is continuously added into the holder by a small injector. It is noted that the fiber is only excited after about 45 seconds from the time THF is added. In this range, THF is well dissolved in water. All measurements are performed at ~298 K.

3. Results and discussions

3.1. WGM lasing microfiber

Figure 2a depicts the power dependent μ-PL spectra from a microfiber with diameter of about 32 μm (optical image attached in the inset). The spectra show a continuous increasing of PL intensity with the increase of PPE. Under the lowest PPE (0.3 μJ), spontaneous emission with a weak broad spectrum can be observed. The broad spectrum changes to sharp peaks under PPE = 0.5 μJ and their intensity increases dramatically with the increase of PPE. These peaks are furthered examined by analyzing the integrated PL intensity as a function of PPE (Fig. 2b). A nonlinear dependence of the integrated intensity on PPE can be observed which indicates a lasing action, and the lasing threshold is determined to be around 0.4 μJ (relates to a fluence per pulse of ~53 μJcm^{-2}).

It was found that lasing wavelengths demonstrate a slightly blue-shift under high PPE [24]. Figure 2c presents the position of primarily lasing peaks denoted as P1 to P4 (Fig. 2a). This phenomenon has been explained in Ref. [31], due to the thermal effect which is nonreversible and hard to avoid in organic materials. However, as can be seen, the value of blue-shift observed in our microfiber is only ~0.1 nm, which is several orders smaller than the previous report (in a range that the excitation power is 7 times larger than the lasing threshold) [24]. This implies the high stability of our microfiber against the thermal effect, which reveals the protection of the active material by the thermally stable polymers, beneficial for steady operation.

WGM lasing is characterized by the polarization (transverse electric (TE) or transverse magnetic (TM)), the angular (m), and the radial momentum numbers (r) [32]. The WGM positions are generally varying for TM and TE modes. Therefore, understanding the polarization of lasing emission is the initial step for analyzing the lasing mechanism. Figures 3a and b plots the schematic diagram of WGMs in TE and TM polarization together with rotation angle of a polarizer. In particular, polarization is TE (TM) when the electric field is perpendicular (parallel) to the fiber-length axis [33]. We analyzed the polarization of lasing spectrum by using the polarizer. At the initial position (rotation angle is zero) the polarizer's axis is parallel to the microfiber as schematically indicated in Figures 3a and b. The integrated PL intensity of a single lasing peak (under a constant excitation) as a function of rotation angle (ϕ) of a polarizer is shown in Fig. 3c. It is clear that the PL intensity fits very well with Malus' law and the polarization is therefore identified to be TM modes only (Fig. 3b).

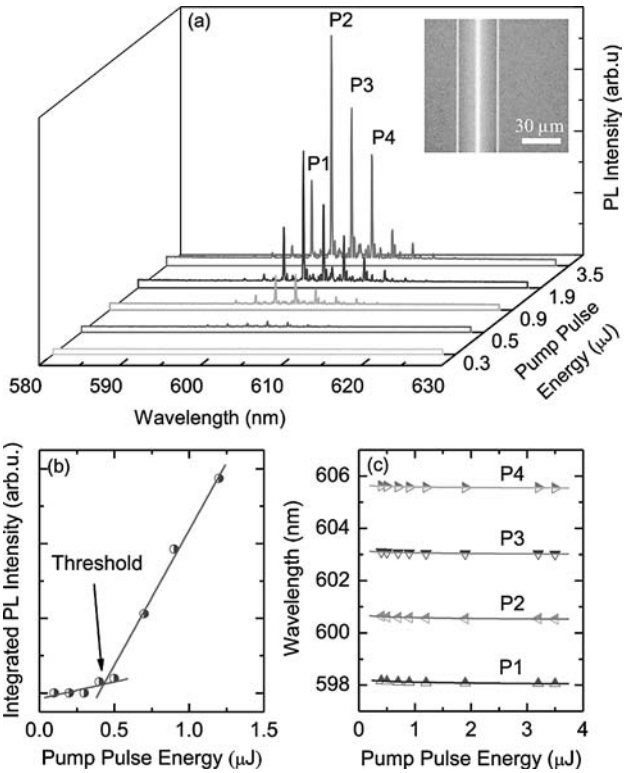

Figure 2 (online color at: www.lpr-journal.org) (a) The PL emission of a typical fiber recorded at room temperature as a function of pump pulse energy. The inset shows the top down view of the microfiber. (b) The integrated PL intensity and (c) Position of lasing peaks (P1–P4) with the pump pulse energy.

Lasing peaks are further examined by using 2D model of WGM theory for TM modes [32, 34]. Let D, n be the diameter and reflective index of the microfiber, respectively. D and n can be estimated from optical image and lasing spectrum. In general, Q factor of a microcavity monotonically decreases with increasing r. Here, only the first ($r = 1$) and the second ($r = 2$) mode orders were taken into consideration since the higher orders have much lower Q factors. The lasing peaks with high intensity are referred to $r = 1$.

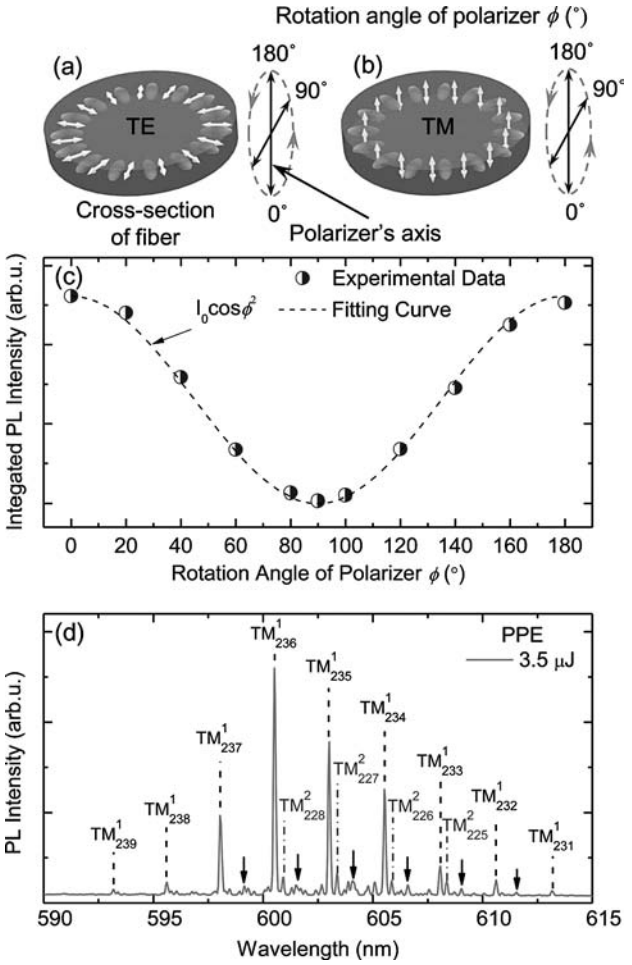

Figure 3 (online color at: www.lpr-journal.org) (a)–(b) Schematic view of WGMs (the ellipsoids) in a microfiber with its electric field oscillation (white arrows) of TE (a) and TM (b). Gradient color in the ellipsoids indicates a field distribution of WGMs which is gradually decreased from the centre to the edge. (c) The integrated PL intensity as a function of rotation angle of polarizer. (d) Mode analysis of the corresponding lasing spectrum. The arrows indicate lasing peaks with mode orders r large than 2.

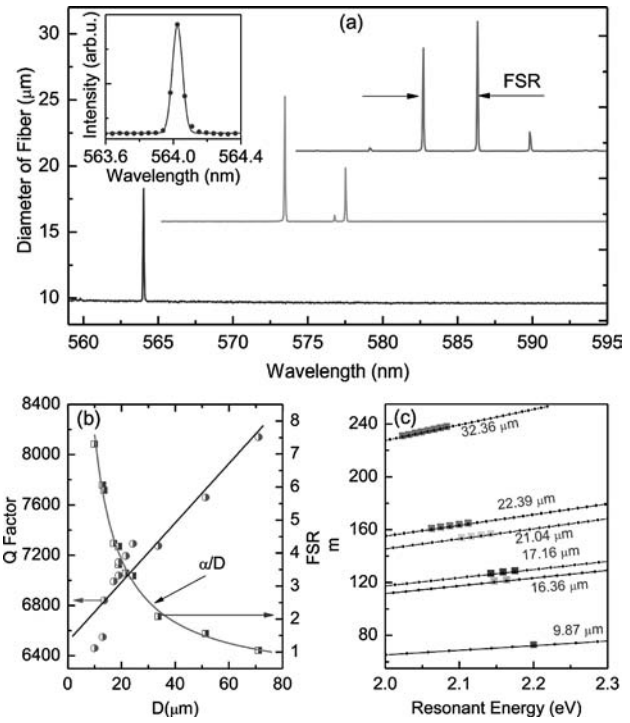

Figure 4 (online color at: www.lpr-journal.org) (a) The μ-PL spectrum of microfibers with different diameters (D), indicated by the baseline value of each spectrum. The inset shows a magnification of the single-mode lasing with the linewidth ($\delta\lambda$) of about 0.085 nm. (b) The FSR and Q factor dependence on microfiber diameters. The FSR curve fits well to a α/D function (α is a constant). (c) Lasing photon energy (large symbols) compared with theoretical data. Diameter of corresponding fibers is shown beside each curve.

Assuming $D = 32.36$ μm (that is close to the estimated value from optical image shown in Fig. 2a), the calculated refractive index of fiber is 1.46, and the corresponding mode numbers m are found to be 231–239. Similarly, the lower peaks are corresponded to second order ($r = 2$), and m are indexed as 225–228. These values matched very well with the lasing peaks in the corresponding spectrum shown in Figure 3c, which therefore confirms the WGM lasing mechanism.

3.2. Size-dependent lasing characteristics

Figure 4a shows a series of lasing spectra from the fibers with different sizes. When D decreases, the number of lasing peaks decreases along with the increase of the free spectral range (FSR). In principle, if the FSR is comparable to the width of optical gain spectrum, single longitudinal mode lasing can be obtained [35]. Following this idea, we has observed single-mode lasing at 564 nm. Linewidth of the lasing mode is ∼0.085 nm, which is much smaller than the linewidth of the previous polymer lasers [36] and nanofiber lasers based on F-P cavity [12, 21]. The obtained narrow linewidth is related to the low optical loss of WGMs. In fact, the emission is confined and selectively enhanced at the circumference of a circular cross-section of the fiber by multiple total internal reflections at the interface between fiber and surrounding medium [23]. Thanks to the extremely low optical loss of the total internal reflection process, the light can travel thousands of cycles before it is coupled outside through elastic scattering. In addition, the calculated lasing mode number is 73 corresponding to $D =$ 9.87 μm. The field distribution inside this microfiber will be presented later.

Subsequently, FSR and Q factor of lasing spectra as a function of D are investigated and presented in Figure 4b. It is noted that the FSR can be described by formula: FSR $= \lambda^2/nL$, where λ is the peak wavelength and L is cavity length. From the value of FSR, L can be calculated and it is found that L is approximately the circumference of microfiber, which once again confirms the WGM lasing mechanism.

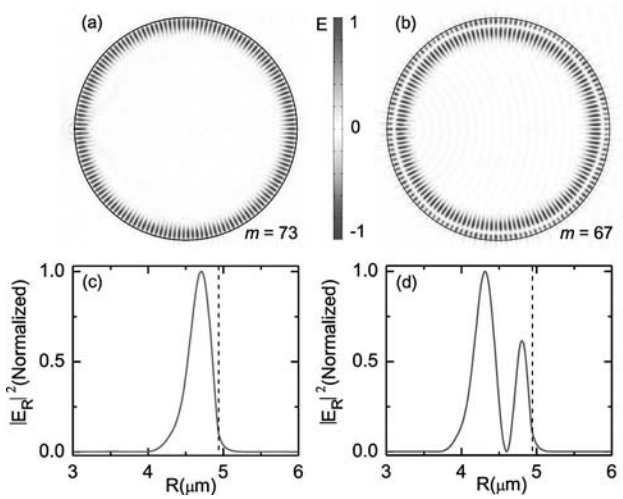

Figure 5 (online color at: www.lpr-journal.org) Normalized magnetic field distribution of TM WGMs in circular cross section of a microfiber ($D = 9.87$ μm, $n = 1.46$) for the first order (a), and the second order (b). The corresponding mode numbers m is indicated at the bottom right corners of the patterns. (c), (d) Normalized field intensity in the radial direction of the first and second orders of TM WGMs, respectively. R is the radius counted from the centre of the fiber. The edge of the fiber is illustrated by dash lines.

Moreover, Q factor (defined as $Q = \lambda/\delta\lambda$, where $\delta\lambda$ is the linewidth of the peak) exhibits a linear increase with increasing D. It can be seen that Q factor is around 6500 for $D \sim 10$ μm to approximate 8200 for $D \sim 71$ μm.

For better comparison between experimental data and theoretical calculation, lasing peak positions from different microfibers as a function of m, together with predicted values are shown in Fig. 4c. The microfiber's diameters used during calculation are very close to corresponding values estimated from optical image. This investigation indicates a good agreement between experimental data (big symbols) and theoretical prediction (line-symbols) for series of microfibers, which supports the WGM lasing mechanism.

3.3. Numerical calculation

Numerical calculation of the electromagnetic field distribution inside the microfiber was carried out. For better demonstration, a typical microfiber with size of 9.87 μm was selected [37] by using the finite element method (supported from COMSOL Multiphysics). Figure 5a presents the field distribution of plane TM wave at resonance wavelength 564 nm inside a circular cross section of the microfiber. From the figure, the first order WGMs (patterns in red and blue color) can be clearly seen together with total internal reflection at the fiber-air interface. It is needed to point out that m, which is equal to the number of field maximum, is found to be 73. This value is exactly the same with the calculated data as mentioned above, therefore, the result is supposed to give a real picture of WGMs. Similarly, Figure 5b shows a possibility of the second order WGMs. In principle, the second order always co-exists with the first order but it has lower Q factor, therefore, higher lasing threshold is expected. As a result, spectrum in Figure 3d shows both the first and the second order modes but with much lower intensities and larger linewidths for second order. It is noted that for a comparable resonant wavelength, the second order has smaller m due to smaller effective cavity length (Figs. 5a and b). In order to get a clearer imagination of the field distribution, intensity profile of the first and the second order WGMs in radial direction are plotted in Figs. 5c and d. It can be easily seen that the field is strongly confined inside the microfiber, while only a small fraction is located outside through evanescent waves. Integration of the distribution curve shows that up to 99% energy is confined inside the fiber for both cases, which should be counted for the low lost WGM lasing observed from the microfibers.

3.4. Refractive index sensing

WGM cavity has been widely used for ultrasensitive biological and optical sensors [38–40]. In principle, evanescent wave of the WGMs, which exist several tens to hundreds of nanometers near the cavity's surface, is very sensitive to even a single molecule [38]. When the evanescent waves interact with molecules from the surrounding medium, a shift of resonance wavelength is indicated [38–40]. In this work, a fiber with $D \sim 36$ μm was used to demonstrate as a refractive index sensor. Figure 6a illustrates our schematic design. In this setup, the fiber is fixed on top of a DBR for low optical loss compared with conventional substrates [29]. Water is served as an environmental medium while certain amount of THF is added to increase the refractive index of the medium. As the refractive index increases, lasing mode should perform a red-shift behavior as shown in Fig. 6b and the shift of resonant peak ($\Delta\lambda$) is expected to be a function of refractive index variation (Δn). We did observe this phenomenon as indicated in Figs. 6c and d by continuously adding THF into the water medium. Refractive index of THF solution is calculated following an experimental work in ref. [41]. In the investigated range, $\Delta\lambda$ is a linear function of Δn, which confirms a validity of the sensing mechanism. Considering this relationship, the sensitivity is as high as 300 nm/RIU. It is important to note that for the fiber inside water (without adding THF) neither blue-shift nor red-shift of lasing mode is observed under excitation with a constant PPE.

In conclusion, we have reported a novel material composition for polymer microfibers fabrication with tunable size, which can be served as high quality optical microresonators and optical sensors. At room temperature, single and multi WGM lasing were observed from the dye-doped microfibers. This achievement is of great significance because microfiber itself can be served as a laser source and waveguide simultaneously for photonic integrated circuits. In fact, the microfibers can be assembled in arrays and ordered structures [12] due to easy fabrication and

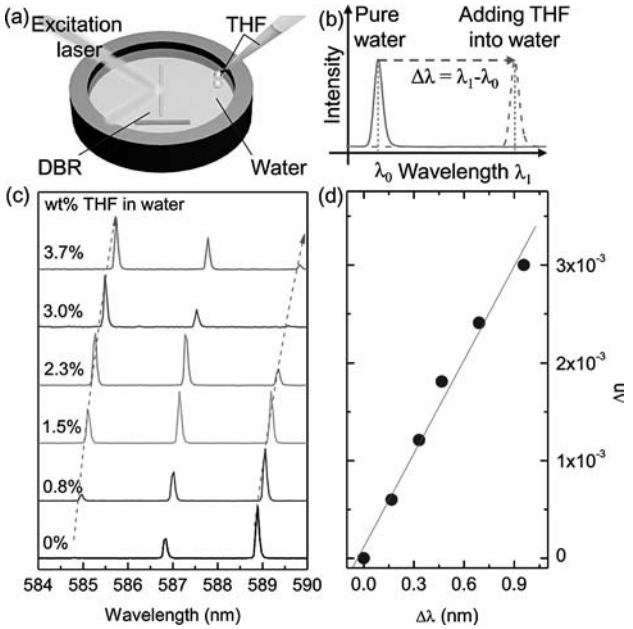

Figure 6 (online color at: www.lpr-journal.org) (a) and (b) Schematic setup and principle of refractive index sensing. (c) Lasing spectra from the studied fiber as a function of THF concentration. (d) Experimental shift of a lasing mode at ∼587 nm ($\Delta\lambda$) versus the refractive index variation of THF solution compared with water (Δn). The experimental data (dots) are well fitted by a linear line, indicating an expected relationship between Δn and $\Delta\lambda$.

mechanical flexibility, therefore, can be served as logic elements [20]. Owing to the doping flexibility, different colloidal quantum dots with wide range emitting wavelength can be introduced by similar technique allowing for wavelength versatility and broad tuning of a laser. In addition, the evanescent wave of the WGMs near the surface of the microfiber was applied for refractive index sensing. This sensing mechanism is very sensitive even to molecules level. Therefore, by constructing more advanced structures such as coupled fibers [40], it is expected to be used for chemical, biological, and optical sensing with much better sensitivity. It is believed that our approach can find extensive potential applications in optoelectronics devices.

Acknowledgements. This research is supported by the National Research Foundation Singapore under its Competitive Research Programme (CRP Award No. NRF-CRP 6–2010–02), and the Singapore Ministry of Education through the Academic Research Fund (Tier 1) under the Project No. RG63/10.

Received: 27 August 2012, **Revised:** 28 September 2012, **Accepted:** 11 October 2012

Published online: 13 December 2012

Key words: Microlasers, whispering gallery modes, microfibers, polymeric materials, refractive index sensing.

Supporting Information: for this article is available free of charge under http://dx.doi.org/10.1002/lpor.201200074

References

[1] R. Chen, D. Li, B. Liu, Z. Peng, G. G. Gurzadyan, Q. Xiong, and H. D. Sun, Nano Lett. **10**, 4956–4961 (2010).
[2] Y. N. Xia, P. D. Yang, Y. G. Sun, Y. Y. Wu, B. Mayers, B. Gates, Y. D. Yin, F. Kim, and Y. Q. Yan, Adv. Mater. **15**, 353–389 (2003).
[3] R. Yan, D. Gargas, and P. Yang, Nat. Photonics **3**, 569–576 (2009).
[4] R. Chen, M. I. Bakti Utama, Z. Peng, B. Peng, Q. Xiong, and H. D. Sun, Adv. Mater. **23**, 1404–1408 (2011).
[5] M. O'Neill and S. M. Kelly, Adv. Mater. **23**, 566–584 (2011).
[6] B. Kang, S. Ko, J. Kim, and M. Yang, Opt. Express **19**, 2573–2579 (2011).
[7] D. Pile, Nat. Photonics **5**, 199–199 (2011).
[8] J. Kameoka and H. G. Craighead, Appl. Phys. Lett. **83**, 371–373 (2003).
[9] D. Li, G. Ouyang, J. T. McCann, and Y. N. Xia, Nano Lett. **5**, 913–916 (2005).
[10] J. M. Moran-Mirabal, J. D. Slinker, J. A. DeFranco, S. S. Verbridge, R. Ilic, S. Flores-Torres, H. Abruna, G. G. Malliaras, and H. G. Craighead, Nano Lett. **7**, 458–463 (2007).
[11] F. Di Benedetto, A. Camposeo, S. Pagliara, E. Mele, L. Persano, R. Stabile, R. Cingolani, and D. Pisignano, Nat. Nanotechnol. **3**, 614–619 (2008).
[12] A. Camposeo, F. Di Benedetto, R. Stabile, A. A. R. Neves, R. Cingolani, and D. Pisignano, Small **5**, 562–566 (2009).
[13] S. A. Harfenist, S. D. Cambron, E. W. Nelson, S. M. Berry, A. W. Isham, M. M. Crain, K. M. Walsh, R. S. Keynton, and R. W. Cohn, Nano Lett. **4**, 1931–1937 (2004).
[14] X. Xing, Y. Wang, and B. Li, Opt. Express **16**, 10815–10822 (2008).
[15] F. Gu, L. Zhang, X. F. Yin, and L. M. Tong, Nano Lett. **8**, 2757–2761 (2008).
[16] H. Zhu, Y. Q. Wang, and B. J. Li, ACS Nano **3**, 3110–3114 (2009).
[17] C. Meng, Y. Xiao, P. Wang, L. Zhang, Y. Liu, and L. Tong, Adv. Mater. **23**, 3770–3774 (2011).
[18] H. Q. Yu, D. W. Liao, M. B. Johnston, and B. J. Li, ACS Nano **5**, 2020–2025 (2011).
[19] K. J. Lee, J. H. Oh, Y. Kim, and J. Jang, Adv. Mater. **18**, 2216–2219 (2006).
[20] M. Hamedi, R. Forchheimer, and O. Inganas, Nat. Mater. **6**, 357–362 (2007).
[21] D. O'Carroll, I. Lieberwirth, and G. Redmond, Nat. Nanotechnol. **2**, 180–184 (2007).
[22] K. J. Vahala, Nature **424**, 839–846 (2003).
[23] M. Humar, M. Ravnik, S. Pajk, and I. Musevic, Nat. Photonics **3**, 595–600 (2009).
[24] H. J. Moon, Y.-T. Chough, J. B. Kim, K. An, J. Yi, and J. Lee, Appl. Phys. Lett. **76**, 3679–3681 (2000).
[25] R. Chen, B. Ling, X. W. Sun, and H. D. Sun, Adv. Mater. **23**, 2199–2204 (2011).
[26] S. V. Frolov, A. Fujii, D. Chinn, Z. V. Vardeny, K. Yoshino, and R. V. Gregory, Appl. Phys. Lett. **72**, 2811–2813 (1998).

[27] M. Kuwata-Gonokami, R. H. Jordan, A. Dodabalapur, H. E. Katz, M. L. Schilling, R. E. Slusher, and S. Ozawa, Opt. Lett. **20**, 2093–2095 (1995).
[28] A. J. Das, C. Lafargue, M. Lebental, J. Zyss, and K. S. Narayan, Appl. Phys. Lett. **99**, 263303–263303 (2011).
[29] V. D. Ta, R. Chen, and H. D. Sun, Adv. Mater. **24**, OP60–OP64 (2012).
[30] A. P. Suryavanshi, J. Hu, and M. F. Yu, Adv. Mater. **20**, 793–796 (2008).
[31] R. Chen, V. D. Ta, and H. D. Sun, Sci. Rep. **2**, 244 (2012).
[32] S. K. Y. Tang, R. Derda, Q. Quan, M. Loncar, and G. M. Whitesides, Opt. Express **19**, 2204–2215 (2011).
[33] R. K. Chang and Y. L. Pan, Faraday Discuss. **137**, 9–36 (2008).
[34] C. C. Lam, P. T. Leung, and K. Young, J. Opt. Soc. Am. B **9**, 1585–1592 (1992).
[35] J. Schäfer, J. P. Mondia, R. Sharma, Z. H. Lu, A. S. Susha, A. L. Rogach, and L. J. Wang, Nano Lett. **8**, 1709–1712 (2008).
[36] L. Persano, P. Del Carro, E. Mele, R. Cingolani, D. Pisignano, M. Zavelani-Rossi, S. Longhi, and G. Lanzani, Appl. Phys. Lett. **88**, 121110–121113 (2006).
[37] C. Czekalla, T. Nobis, A. Rahm, B. Cao, J. Zúñiga-Pérez, C. Sturm, R. Schmidt-Grund, M. Lorenz, and M. Grundmann, Phys. Status Solidi B **247**, 1282–1293 (2010).
[38] F. Vollmer and S. Arnold, Nat. Methods **5**, 591–596 (2008).
[39] M. A. Santiago-Cordoba, S. V. Boriskina, F. Vollmer, and M. C. Demirel, Appl. Phys. Lett. **99**, 073701 (2011).
[40] S. I. Shopova, Y. Sun, A. T. Rosenberger, and X. Fan, Microfluid. Nanofluid. **6**, 425–429 (2009).
[41] T. M. Aminabhavi and B. Gopalakrishna, J. Chem. Eng. Data **40**, 856–861 (1995).